

RELICT OLIVINES IN MICROMETEORITES: PRECURSORS AND INTERACTIONS IN THE EARTH'S ATMOSPHERE

N. G. Rudraswami^{1*}, M. Shyam Prasad¹, S. Dey^{1,2}, D. Fernandes¹, J. M. C. Plane³, W. Feng³, S. Taylor⁴, J. D. Carrillo-Sánchez³

¹National Institute of Oceanography (Council of Scientific and Industrial Research), Dona Paula, Goa 403004, India

²Indian Institute of Technology, Roorkee, Uttarakhand 247667, India

³School of Chemistry, University of Leeds, Leeds LS2 9JT, UK

⁴Cold Regions Research and Engineering Laboratory, 72 Lyme Road, Hanover, New Hampshire 03755-1290, USA

Corresponding Author: rudra@nio.org

ABSTRACT

Antarctica micrometeorites (~1200) and cosmic spherules (~5000) from deep sea sediments are studied using electron microscopy to identify Mg-rich olivine grains in order to determine the nature of the particle precursors. Mg-rich olivine (FeO < 5wt%) in micrometeorites suffers insignificant chemical modification during its history and is a well-preserved phase. 420 forsterite grains enclosed in 162 micrometeorites of different types - unmelted, scoriaceous and porphyritic - are examined in this study. Forsterites in micrometeorites of different types are crystallized during their formation in solar nebula; their closest analogues are chondrule components of CV-type chondrites or volatile rich CM chondrites. The forsteritic olivines are suggested to have originated from a cluster of closely related carbonaceous asteroids that have Mg-rich olivines in the narrow range of CaO (0.1–0.3 wt%), Al₂O₃ (0.0–0.3wt%), MnO (0.0–0.3wt%) and Cr₂O₃ (0.1–0.7wt%). Numerical simulations carried out with the Chemical Ablation Model (CABMOD) enable us to define the physical conditions of atmospheric entry that preserve the original compositions of the Mg-rich olivines in these particles. The chemical compositions of relict olivines affirm the role of heating at peak temperatures and the cooling rates of the micrometeorites. This modelling approach provides a foundation for understanding the ablation of the particles and the circumstances in which the relict grains tend to survive.

1. INTRODUCTION

Extraterrestrial dust particles in sizes ranging from tens of μm to a few mm originate from two likely sources: a) the asteroid belt where the dust is generated from collisions between large bodies; and b) cometary bodies releasing dust due to solar heating during their perihelional passage (Brownlee 2001). The understanding of the specific types of source that contribute to the dust is still evolving. There is general disagreement among researchers whether a large component comes from the asteroid belt or from cometary bodies (Brownlee 2001; Kortenkamp et al. 2001; Nesvorný et al. 2010, 2011). However, the Zodiacal Cloud (Nesvorný et al. 2010, 2011) considers the Jupiter Family of Comets as the main contributor, with minor contributions from the Asteroid belt and the Halley type comets. The larger orbital eccentricities do not allow cometary particle to get confined to the Earth's resonance orbit (Dermott et al. 1994; Reach et al. 1997; Brownlee 2001). Cometary dust has much higher entry velocity than asteroidal dust and in the process loses the gravitational focusing required to be captured by the Earth (Flynn, 1989). In addition, the cometary particles that got trapped in the Earth's resonance orbit will have high entry velocities and undergo large scale ablation during atmospheric entry thereby losing their properties and identity (Flynn 1989a,b; Brownlee 2001; Kortenkamp et al. 2001). On the other hand, the gravitational focusing is more in asteroidal dust and these particles enter the Earth's resonance orbit at much lower velocities (Flynn 1989a,b). Moreover, the collision between asteroids generates large amount of dust that swarm into the resonance orbit of the earth. It is estimated that of the $\sim 30,000$ tons/annum of meteoroids that enter the Earth's atmosphere (Love and Brownlee, 1993; Peucker-Ehrenbrink and Ravizza 2000; Plane 2012), only ~ 3000 tons/annum reaches the surface, of which large percentage of the particles undergo heating and are chemically altered losing their distinctive properties, which otherwise could have led to understanding of the precursors (Taylor et al., 1998, 2007). The new estimates of micrometeorites accretion rate ~ 16000 tons/annum was suggested based on micrometeorites collected from Antarctica and noble gas measurements done on residue (Yada et al. 2004). The model for the zodiacal cloud also corroborate the above new estimates (Nesvorný et al. 2011).

Much information on micrometeorites can be acquired from relict grains preserved in the particles that have escaped significant atmospheric heating. The relict grains, especially those composed of Mg-rich olivine with an FeO content $< 5\text{wt}\%$, are markedly different from other grains in the same micrometeorite. Mg-rich olivines are dominant in large numbers of micrometeorites. Investigating the nature of relict grains is therefore useful for identifying the range of chondrites that contributes to the flux of micrometeorites (Steele, 1985a,b; Steele, 1992). The survival of the relict grains also

constrains the temperature the particle may have experienced during atmospheric entry. Mg-rich relict grains are commonly found in chondrules and fragments embedded in the matrix of carbonaceous chondrites, but rarely in ordinary chondrites. Identification of relict olivine is therefore an important link to a particle's thermal history during atmospheric entry, as well as the precursor meteoroid. We therefore confine our discussion to the understanding of precursors and atmospheric entry parameters that facilitate survival of the grains. The composition of minor elements present in the relict mineral helps narrow down the precursor with greater precision than the bulk chemical composition (Steele, 1985a, b; 1992), particularly because Mg-rich olivine can be compared with Mg-rich olivine in chondritic components. In contrast, the bulk chemical composition of a particle may alter depending on the heating experienced during atmospheric entry, and is typically close to CI composition (Kurat et al., 1994; Brownlee et al., 1997; Taylor et al., 2000; Rudraswami et al., 2012, 2014). Earlier studies were limited by statistics due to the small number of relict grains analyzed (Steele, 1985a, b; 1992). The present comprehensive study with a larger number of samples allows us to make a stronger case for understanding the nature of the precursor.

The forsteritic olivine of micrometeorites collected from Antarctica and deep sea sediments has been studied previously to discern the nature of the precursor and its behaviour during atmospheric entry (Taylor et al., 1998, 2000; Prasad et al., 2013, 2015). However, in the present study we will use the Chemical Ablation Model (CABMOD, Vondrak et al., 2008) to understand the ablation of major and minor elements and the thermal history that a meteoroid of specified mass, velocity and entry angle undergoes during flight through the atmosphere before landing on the Earth's surface as a micrometeorite. CABMOD takes into account sputtering of atoms by high velocity inelastic collisions with air molecules, followed by the onset of particle melting which leads to the more rapid evaporative loss of atoms and oxides as a function of altitude.

2. SAMPLE COLLECTION AND ELECTRON MICROSCOPY

The samples were collected from Antarctica and Deep sea sediments using different collection techniques. The Antarctica micrometeorites (AMM) were collected from the South Pole Water Well (SPWW) which has a diameter of ~24 m at a depth of ~100 m below the snow surface, with a total water volume of ~5000 m³ (Taylor et al., 1998, 2000). The cosmic spherules from deep sea sediments (CS-DSS) were collected at water depths of ~5200 m using an Okean grab sampler with a seafloor penetration depth of ~15 cm (Rudraswami et al., 2012, 2014, 2015a; Prasad et al., 2013). The AMM and CS-DSS have been dated at ~900 years BP and 0–50,000 years BP, respectively (Taylor et al., 2007, 1998; Prasad et al., 2013). The samples were mounted in epoxy and were

gradually ground until the particles were sectioned diametrically. The CS-DSS were initially size sorted under a binocular microscope so that while grinding all samples received equal area exposure and no small sized samples were lost due to over polishing to expose larger-sized samples. One epoxy section of AMM was mounted with ~1200 particles, while 27 epoxy mounts were prepared for the deep sea spherules that accommodated ~5000 particles to scan for Mg-rich olivines (Fo >95%).

Each particle was examined in detail using back scattered electron (BSE) images obtained by a JEOL JSM 5800LV SEM with an OXFORD INCA Energy Dispersive Spectrometer detector (EDS, ISIS-300), in order to identify systematically the Mg-rich mineral phases. These were further analyzed using a Cameca SX5 Electron Micro Probe Analyzer to obtain the chemical composition. Selected minor elements were analyzed for longer counting times to improve the detection limits. Multiple analyses were done on most of the relict olivine grains (depending on the grain size); these analyses were then averaged. Both electron microscopy instruments are housed at the National Institute of Oceanography (NIO), Goa.

3. RESULTS

Relict olivine are Mg-rich olivine (Fo >95%) grains that are not formed from crystallization during atmospheric entry. They are distinctive in the spherule and can be easily identified from their large grain size, morphology, chemical composition and many times associated with presence of Fe, Ni-metals enclosed within these grains. Mg-rich olivines are largely found in unmelted, scoriaceous and porphyritic micrometeorites. Nearly ~5000 particles from AMM and CS-DSS were examined using BSE images and EDS to recognize Mg-rich olivines which were then further analyzed with the electron microprobe to understand the variability of their chemical composition and the nature of the precursors contributing to these micrometeorites. CS-DSS particles have to survive the harsh seafloor conditions, which suggests that the more fragile particles have fallen recently. CS-DSS have Mg-rich olivines that are of relatively small sizes so that large numbers of specimens had to be scanned under the SEM to collect a sizeable number of Mg-rich olivines. AMM usually have larger forsteritic olivines occurring in greater numbers. The selected Mg-rich olivines are angular in shape with no textural alteration, and typically occupy a large area of the spherule. Representative BSE images of micrometeorites which contain relict olivines, collected from SPWW and DSS, are shown in Fig. 1.

Although olivine grain has a wide range in composition, we consider here a narrow range of forsteritic composition (Fo = 95–100%). The bulk chemical composition of the spherules are significantly different from that of the Mg-rich olivine, with high Al, Ca, Fe and Ni abundances. We

selected 182 olivine grains from 63 AMM, and 238 grains from 162 CS-DSS, to provide useful statistical control on the types of precursors. All Mg-rich olivines are collected as part of systematic study to understand the distribution of minor elements. A majority of the relict olivines from AMM and CS-DSS have Cr₂O₃, MnO, CaO ranging from 0.1–0.7 wt%, 0.0–0.3 wt%, 0.1–0.3 wt%, respectively (Fig. 2 & 3). The relict olivines in micrometeorites collected from Antarctica and deep sea sediments show similar patterns. The bulk chemical composition of particles from AMM and CS-DSS was determined using the Lispix software program, which shows that the major element compositions are close to CI-chondrites. Some unmelted particles or single grains from AMM deviate from the CI values (Rudraswami et al., 2015a). The minor elements in Mg-rich olivine behave as follows: CaO correlates with Al₂O₃ (**Fig. 2a, 3a**), and CaO seems to anti-correlates with Cr₂O₃ and MnO (**Fig. 2b, 2d, 3b, 3d**), as with increase of CaO there is decrease of Cr₂O₃ and MnO; Cr₂O₃ correlates with MnO (**Fig. 2c, 3c**); and FeO seems to correlate with MnO and Cr₂O₃ (**Fig. 2e, 2f, 3e, 3f**). There is a slight spread in the FeO data as this oxide have been affected to some extent during atmospheric entry. The size (diameter in μm) of the micrometeorites, size (length and breadth in μm) of relict grain, and chemical composition of the relict olivine grain are provided in Appendix A and Fig. 4. There are some micrometeorites that are single mineral and hence the relict grain sizes are comparable to size of micrometeorites itself. Some micrometeorites with relict grain have irregular external shape, in such circumstance we have reported the maximum length (μm) of the particle.

4. DISCUSSION

4.1. Relict olivine in micrometeorites

The presence of relict grains in many micrometeorites indicates that the grains did not re-crystallize during their high temperature atmospheric entry, but are preserved from their original formation (Genge et al. 2008). The forsterites in micrometeorites are not in equilibrium with the surrounding melt during atmospheric entry and may not have crystallized from the spherule composition that is Fe-rich. The forsterites have escaped melting as they are more refractory and were heated for a short time during atmospheric entry, so that the relatively large relict grains were not resorbed into the molten material. Heating followed by fast cooling therefore retained the minor chemical components in the grains, which would otherwise have easily diffused away. These grains are the basic components of the chondrules from which they have apparently formed (Steele, 1986, 1992; Brearley and Jones, 1998; Wasson and Rubin, 2003; Hewins et al., 2005; Jones and Carey, 2006), so that the forsterite provides significant clues about precursors to the flux of micrometeorites.

The present discussion is centred on understanding what types of precursors contribute to the Mg-rich grains in micrometeorites, and a comparison is made with the existing data for C1 (CI), C2 (CM) and C3 (CV) chondrites (Steele, 1986, 1990; Rubin and Wasson, 1986; Kurat et al., 1989; Jones and Carey 2006; Russell et al., 2010; Rudraswami et al., 2011). Olivine is the dominant phase in chondrules, namely type I (FeO poor with Fa<10%) and II (FeO rich with Fa>10%), and the olivine varies in composition from Mg-rich to Mg-poor (Hewins, 1997). Mg-rich olivines are common in type I chondrules that are abundant (>90%) in all types (CM, CO, CV, CR) of carbonaceous chondrites (CCs) (Scott et al., 2005). Unequilibrated ordinary chondrites (UOCs) rarely contain Mg-rich olivine. The chondrules that are surrounded by fine-grained matrix are dominated by Fe-rich olivine. The Mg-rich forsterites represent chondrule precursors that are not thermally altered and have witnessed and survived the chondrule forming event (Jones et al., 1996). The Mg-rich olivines are supposed to be the major silicates in chondrules formed from the high temperature condensate in a stellar outflow, and are the early major condensate (Steele, 1986). The minor elemental composition of Mg-rich olivines in CCs allows the Mg-rich olivine of chondrules and its components to be compared. In the present study we have compared Mg-rich olivine from chondrules of CI (Orgueil and Tagish lake), CM (Murchison and Yamato 82042) and CV3 (Allende and Mokoia) chondrites. The minor elements such as MnO, CaO, Al₂O₃ and Cr₂O₃, and the FeO in Mg-rich olivine of C1 chondrites are indistinguishable from those of C2, hence it may be difficult to narrow down based on the chemistry (Steele, 1985a, 1990, 1992). The olivines in CI are small, rare and are embedded in matrix, hence we do not consider CI-chondrite to be contributing to relict bearing particles. The olivine in the chondrules of UOCs has a forsterite content pre-dominantly in the range of 70–90%. The olivines in UOCs also have a low CaO content, hence an insignificant number of micrometeorites can be related to ordinary chondrites (Beckerling and Bishcoff, 1995). **The above conclusion is also supported by oxygen isotopic studies on relict olivine in micrometeorites that fall in the range of chondrule from carbonaceous chondrites rather than ordinary chondrites (e.g. Rudraswami et al., 2015b, 2016).**

Forsteritic olivines in CI chondrites are rare and small in size (Steele, 1990), and are closely associated with CM rather than CV chondrites (Steele, 1985, 1990). Henceforth data from the present study are compared only with CM and CV chondrites. The general data suggest relict bearing micrometeorites are strongly correlated with the CV chondrule data, but there are certain regions that are common to both CM and CV data. The data overlap with the C2 and C3, as suggested by Steele (1985a, b). The majority of the forsterites in CV chondrules have Cr₂O₃ and MnO contents confined to narrow ranges of 0.0–0.3 wt% and 0.0–0.1 wt%, respectively. The ranges in CM chondrules are

0.0–0.8wt% and 0.0–0.3 wt%, respectively. The forsterites in most micrometeorites fall close to the CM region. This is also true for the CaO versus Cr₂O₃ and MnO plots (Figs. 2 and 3). Earlier work done by Steele (1985a, b; 1992) analyzed a small number of olivines (total of ~64) for different studies. They concluded that micrometeorites are largely related to C2 chondrites, with some contribution of C3 and UOC type chondrites. An overwhelming majority of forsterites from micrometeorites in the present study cluster in the narrow range shown by the rectangles in Figs. 2 and 3, displaced slightly from C3 data and displaying an affinity to C2 forsterites, though not completely. The observation of clustering of the data is statistically significant as it points towards the possibility that the micrometeorites largely originate from a group of asteroids that have forsteritic chemical composition lying in a restricted range. **These type of asteroid would be fragile or enriched in regolith layer, thereby producing larger amount of dust particles into interplanetary space during collision.** Among the chondrules, type I in C2 and C3 contribute up to ~90%, while the remaining ~10% are of type II (Jones, 2012). The large size of the forsterites in the present study is also suggestive of their derivation from the type I chondrules in C2 and C3 which have a high abundance of forsterites that are large in size. Overall, the forsterites seem to be parts of the chondrule precursor material and have not been recycled during chondrule formation and later during incorporation into parent bodies. These grains may have escaped catastrophic collisions in the asteroid belt followed by atmospheric entry heating. Some forsterites have small fayalitic rims (~few μm) which appear to have formed due to rapid alteration during their high temperature transit while entering the atmosphere, followed by fast cooling. This process essentially preserved the forsteritic cores. **The relict bearing, scoriaceous and porphyritic spherules have not experienced temperature greater than 1700 K during atmospheric entry. Hence the large-sized forsterite grains of these spherules does not seem to be in equilibrium with the FeO-rich surroundings from less than a few percent present in the core of the relict grain to as high as 10–30% on the rim** within the timeframe of atmospheric heating. A slow heating and cooling rate would have allowed FeO to diffuse into the forsterite and resulted in a loss of forsteritic identity. Another way would be to heat the meteoroid above 1900 K so that it completely melted. The atmospheric heating constraints related to the survival of the relict forsterite grains are discussed in next section.

4.2. Temperature, size and entry angle

Extraterrestrial particles preserve the properties of the precursors and provide information that enhances our understanding of the solar system provided the chemical compositions are intact and not altered during atmospheric entry. We explore the physical and chemical processes of the

fragments of dust particles that have been incorporated in the Earth resonance orbit based on various entry parameters. Numerical calculation was done using CABMOD model to examine the change in the chemical composition of the incoming particles as a function of mass, velocity, entry angle with respect to the zenith (ZA), and particle density (Vondrak et al., 2008). This involved exploring the parameter space of these variable to determine the conditions under which relict grains would survive atmospheric entry. The principal goal of earlier model studies was to look into ablation of the particles and the temperature experienced during various entry velocities (Flynn 1989a, b; Love and Brownlee, 1991). CABMOD determines the ablation rates of individual elements (Mg, Fe, Si, Ca, Al, Ti, Na and K) along the meteor track from an initial altitude of 500 km. In the present study we also consider the amount of time the particle remains within 100 K of the peak temperature, the cooling rate, and the deviation from initial chemical composition of the particle during its journey through the upper atmosphere. For these model runs, a CI composition is used with a particle density of 2 g/cm^3 (Vondrak et al., 2008; Mason 1971; Sears and Dodd 1988; Lodders and Fegley 1998). The present study consider the smallest particle size of $\sim 100 \text{ }\mu\text{m}$ in diameter that we can work with comfortably and the largest size of $\sim 700 \text{ }\mu\text{m}$. It should be noted size of particle is synonym to diameter of particle. Larger size particles (diameter $>$ ca. $100 \text{ }\mu\text{m}$) can undergo extensive melting and vaporization depending on the ZA and entry velocity. Here we have restricted the entry velocity 16 km/s , beyond which the particles (sizes ranging from 100 to $700 \text{ }\mu\text{m}$) lose substantial mass and undergo significant compositional change (Rudraswami et al., 2015b).

The particle ZA has a large effect on the thermal profile during entry. Entering at $ZA = 0^\circ$, a particle will heat and cool faster than when entering at the grazing angle ($ZA = 90^\circ$). The time the particle remains within 100 K of the peak temperature varies from 0.5 to 1 s, depending on the ZA and size of the particle. Larger particles spend less time close to the peak temperature compared to smaller particle entering with the same ZA and velocity.

A cooling rate of $\sim 300\text{--}500 \text{ K/s}$ for any ZA means that the particle temperature drops rapidly below 600 K within a few seconds. Thus, the heating up to the peak temperature **of $<1700 \text{ K}$ in relict bearing**, scoriaceous and porphyritic particles should not cause changes in the initial composition of relict forsteritic grains, in contrast to the bulk chemical composition which is altered by ablation (Fig. 2–3). This is not the only parameter that is paramount, it is also concomitant with entry mass and velocity. Particles of diameter less than $200 \text{ }\mu\text{m}$ and entry velocity 11 km/s undergo ablation of only few percent at any ZA ; however, as size increases only those particles that enter at high ZA

(70–90°) are well preserved (Fig. 5). Conversely, for 16 km/s, particle ablation is high for small size particles (~100 μm), apart from an even narrower range of ZA (80°–90°) (Fig. 5).

The bulk Ca/Si (atomic) and Al/Si (atomic) ratios are close to the solar composition irrespective of the type of cosmic spherule (Rudraswami et al., 2015b). However, Mg-rich olivine is different from the bulk chemical composition of the particle. Even if the spherule has experienced a temperature as high as 1700 K, Mg-rich olivine will escape chemical alteration due to its large size and brief heating time during atmospheric entry. Such grains potentially record the original composition when they formed in solar nebula. Two different entry velocities of 11 and 16 km/s are considered in the present study, as with faster particles complete ablation occurs (Vondrak et al., 2008; Rudraswami et al., 2015b).

The first stage of heating results in loss of Fe followed by Si and Mg, which is the reason for the increase in the Mg/Si ratio (Hashimoto, 1983; Rudraswami et al., 2015b). The Fe loss is too large compared to other major elements like Si and Mg, resulting in increase in Ca and Al (Fig. 6–7). The ternary Mg-Fe-Si plot in Fig. 8 illustrates how the loss of Fe varies as a function of size, ZA and velocity. The loss of Fe results in a relative increase in Si and Mg, which changes the bulk chemical composition from olivine stoichiometry to that of pyroxene (Hashimoto, 1983). Ablation of the refractory elements such as Ca, Al and Ti depend on the particle mass, ZA and entry velocity (Fig. 7). The ablation of these elements is negligible for a velocity of 11 km/s irrespective of the size and ZA, even when the major elements Si, Mg, Fe have largely ablated (Fig. 6). At 16 km/s, the refractory elements like Ca, Al, Ti do not show ablation for particles sizes less than 400 μm irrespective of ZA, but there is large scale ablation for Si, Mg and Fe (Fig. 7). Al is the most robust of these elements for those sizes followed by Ca and Ti. Ti ablates by a few percent for smaller sizes at ZA < 50°; Ca ablation starts for particles greater than ~400 μm and rises rapidly beyond 500 μm . Al does not undergo ablation for any zenith angle for ~450 μm and rises slightly to only a few percent at 600 μm , for ZA < 30°. For most of the micrometeorites analysed, whose size is below 300 μm , Ca and Al have most likely undergone no ablation, and Ti only a small amount (Fig 7). This suggests that the chemical composition of the minor refractory elements will have been preserved even after the particle has been heated to ~1700 K irrespective of the ZA, although the particle undergoes large scale vaporization of Si, Mg, Fe thereby unbalancing the chemical composition (Fig. 6–8).

For an entry velocity of 16 km/s there is a limited range of ZA for which the total ablation is less than 20%. For a 200 μm particle the ZA is > 65°, while for a 300 μm particle ZA > 70°. For ZA =

70–80°, the temperature reaches ~1700 K resulting in ablation of ~1–8% in the size range of the micrometeorites we have analyzed (Rudraswami et al., 2015b). The small olivine grains at these temperatures will have mobilized elements, but the large-sized forsterites are temperature resistant, as is obvious from the behaviour of their chemical compositions (Fig. 2–3). Faster cooling has also prevented diffusion to the neighbouring phases. At very high ZA (80–90°), there is a smooth entry with no ablation. Overall, a ZA > 65° is ideal for a particle size up to ~200 µm, since the relict olivine will be retained in its original chemical composition. However, particles larger than 300 µm will experience a temperature above liquidus state (>1900 K) for a relatively long time (**less than few seconds**) depending on the ZA and entry, as it penetrates deeper into atmosphere, so that relict minerals will tend to lose their identity and homogenize with the bulk chemical composition. As the ZA goes on increasing the given size particle will spend more time at peak temperature. In general, the time spent at peak temperature where most particle attain liquidus temperature will be less than 1 s and 2 s for 11 and 16 km/s, respectively. The AMM has size range from ~50–200 µm, while that of CS-DSS has size range from ~150–400 µm and few beyond. The histogram plot in Fig. 4 indicates AMM and CS-DSS has peak of ~100 µm and 220 µm, respectively. The majority of the relict grain have size range ~10–40 µm irrespective of micrometeorite size range (Fig. 4). The large size relict grain is from the single mineral micrometeorite where the ablation of the micrometeorite is much smaller with no change in chemical composition. The entry velocity of 11 km/s and ZA=65°, the micrometeorites with sizes from ~50–400 µm will be perfect for preserving relict grain as the volatile element Fe does not get ablated. On the other hand, for entry velocity at 16 km/s to preserve the relict grain with chemical composition the range of ZA is ~70–90° for micrometeorites sizes <100 µm, ZA>75° for ~100–200 µm and ZA=80–90° for sizes >200 µm. The relict bearing particles which are decisive in revealing the precursor of the particles they belong to have a strict entry parameters in term of entry velocity, ZA and size as discussed above.

5. CONCLUSIONS

Mg-rich olivine (Fo>95%) in AMM and CS-DSS is unusual and can be easily distinguished from the neighbouring grains. The Fo-rich grains and their chemical composition suggests that the high temperatures experienced by the meteoroid during atmospheric entry has not altered the minor elemental compositions of these olivines. The forsterites that are widespread in chondrules and also found in micrometeorites, which suggests a major contribution from chondrule components of CCs like CV chondrules and forsterites from CM chondrites, rather than CI chondrites. The composition

data of the Mg-rich olivines indicate frequent collisions between a similar group of asteroids that generated dust having Mg-rich olivines in a narrow range of Al₂O₃, CaO, MnO and Cr₂O₃ relative abundances, slightly different from CM and CV carbonaceous chondrites. The systematic deviation of the bulk composition suggests that relict grains in scoriaceous and porphyritic micrometeorites are more resistant to the heating experienced by micrometeorites. The CABMOD simulations indicate that particles smaller than 300 µm with entry velocities less than 16 km/s and large ZA (70–90°) ° are likely to preserve the relict minerals.

Acknowledgements

This work is supported by the CSIR XII Plan funded Project GEOSINKS and the PLANEX project, Physical Research Laboratory, Ahmedabad (NGR and MSP). We thank Vijay Khedekar for his support in EPMA and electron microscopy. The CABMOD model development is supported by the European Research Council (project 291332—CODITA). The National Science Foundation funded the collection of micrometeorites from the South Pole water well. This is NIO's contribution No. xxxx.

REFERENCES

- Brearley, A. J., & Jones, R. H. 1998, in *Reviews in Mineralogy*, Vol. 36, Planetary Materials, ed. J. J. Papike (Washington: Mineral. Soc. America), chap. 3
- Brownlee D. E. 2001, *Acretion of Extraterrestrial Matter Throughout Earth's History* (eds. B. Peucker-Ehrenbrink and B. Schmitz), pp. 1–12. Kluwer/Plenum, New York.
- Brownlee D. E., Bates B. & Schramm L. 1997, *M&PS* 32, 157
- Dermott S.F., Jayaraman S, Xu. Y. L., Gustafson B. A. S. & Liou J. C. 1994, *Nature* 369, 719
- Flynn G.J. 1989a, *Proc. LPSC*. 19, 673
- Flynn G.J. 1989b, *Icarus* 77, 287
- Genge M. J., Engrand C., Gounelle M. & Taylor S. 2008, *M&PS* 43, 497
- Hashimoto A. 1983, *Geochem. J.*, **17**, 111
- Hewins R. H., Connolly H. C., Lofgren G. E. Jr., & Libourel G. 2005, In *Chondrites and the protoplanetary disk*, edited by Krot A. N., Scott E. R. D., and Reipurth B. ASP Conference Series, vol. 341. San Francisco: Astronomical Society of the Pacific. 286 p.
- Jones R. H., in: R. Hewins, R. Jones, E. Scott (Eds.), *Chondrules and the Protoplanetary Disk*, Cambridge University Press, Cambridge, 1996, pp. 163–172
- Jones R. H. 2012, *MAPS*, 47, 1176

- Jones, R. H., & Carey E. R. 2006, *Am. Mineral.*, 91, 1664
- Kortenkamp S. J., Dermott S. F., Fogle D., & Grogan K. 2001, Accretion of Extraterrestrial Matter Throughout Earth's History (eds. B. Peucker-Ehrenbrink and B. Schmitz), pp. 13–30. Kluwer/Plenum, New York.
- Kurat G., Koeberl C., Presper T., Brandstätter F., & Maurette M. 1994, *GCA*, **58**, 3879
- Kurat G., Mayr M., Ntaflos Th. & Graham A. L. 1989, *Meteoritics*, **24**, 35
- Lodders K. & Fegley B. Jr. 1998, *The Planetary Scientist's Companion*. Oxford University Press, New York.
- Love S. G. & Brownlee D. E. 1991, *Icarus* 89, 26–43.
- Love S. G. & Brownlee D. E. 1993, *Science* 262, 550
- Mason, B. (1971) *Handbook of Elemental Abundances of the Elements in Meteorites*, Gordon and Breach, Newark, USA.
- Nesvorný, D., Janches, D., Vokrouhlický, D., Pokorný, P., Bottke W. F., & Jenniskens, P. 2011, *ApJ*, 743, doi:10.1088/0004-637X/743/2/129
- Nesvorný, D., Jenniskens, P., Levison, H. F., Bottke, W. F., Vokrouhlický, D., & Gounelle, M. 2010, *ApJ*, 713, 816
- Peucker-Ehrenbrink B. and Ravizza G. 2000, *GCA*, 64, 1965
- Plane J. M. C. 2012, *Chem. Soc. Rev.* 41, 6507
- Prasad M. S., Rudraswami N. G. & Panda D. K. 2013, *JGR*, **118**, 2381
- Prasad M. S., Rudraswami N. G., Araujo A., Babu E. V. S. S. K. & Vijaya Kumar T. 2015, *MAPS*, **50**, 1013
- Reach W. T., Franz B. A, Weiland J. L. 1997, *Icarus*, **127**, 461–484.
- Rubin A. E. and Wasson J. T. 1986, *GCA*, 50, 307
- Rudraswami N. G., Prasad S. M., Plane J. M. C., Berg T., Feng W. & Balgar S. 2014, *GCA*, **131**, 247
- Rudraswami N. G., Shyam Prasad M., Babu E. V. S. S. K., Vijaya Kumar T., Feng W. & Plane J.M.C. 2012, *GCA*, **99**, 110, 78
- Rudraswami N. G., Shyam Prasad M., Dey S., Plane J. M. C., Feng W. & Taylor S. 2015a, *APJ*, **814**, doi:10.1088/0004-637X/814/1/78
- Rudraswami N. G., Shyam Prasad M., Nagashima K., & Jones R. H. 2015b, *GCA*, **164** , 53
- Rudraswami N. G., Shyam Prasad M., Jones R. H., & Nagashima K. 2016, *GCA*, <http://dx.doi.org/10.1016/j.gca.2016.08.024>**
- Rudraswami N.G., Ushikubo T., Nakashima D., Kita N.T. 2011, *GCA*, **75**, 7596

- Russell S. D. J., Longstaffe F. J., King P. L., & Larson T. E. 2010, *GCA*, 74, 2484
- Scott E.R.D., Krot A.N., Chondrites and their components, in: A.M. Davis (Ed.), *Meteorites, Comets, and Planets, Treatise on Geochemistry*, Elsevier, Amsterdam, 2005, pp. 143–200.
- Sears, D. W. and Dodd, R. T. 1988 in: *Meteorites and the Early Solar System*, edited by: Kerridge, J. F. and Matthews, M. S., University of Arizona Press, Tucson, 3–31
- Steele, I. M. 1986, *GCA*, 50, 1379
- Steele, I. M. 1986, *GCA*, 56, 2923
- Steele, I. M. 1990, *Meteoritics*, 25, 1990
- Steele, I. M., Smith, J. V. & Brownlee, D. E. 1985b, *Nature*, 313, 297
- Steele, I. M., Smith, J. V. & Skirius, C. 1985a, *Nature*, 313, 294
- Taylor S., Lever J. H. & Harvey R. P. 2000, *M&PS*, **35**, 651
- Taylor, S., Lever, J. H. & Harvey, R. P. 1998, *Nature*, **392**, 899
- Taylor, S., Matrajt, G., Lever, J. H., Joswiak, D., & Brownlee D. 2007. Size distribution of Antarctic Micrometeorites, in *Dust in Planetary Systems* (ed. H. Krüger, and A. Graps) ESA Publications, SP-643, 145-149.
- Vondrak T., Plane J. M. C., Broadley S. & Janches D. 2008, *Atmos. Chem. Phys.*, **8**, 7015
- Wasson, J. T., & Rubin, A. E. 2003, *GCA*, 67, 2239

FIGURES CAPTION

Figure 1.

Representative back-scattered electron images of relict bearing Antarctica (a–c) and Deep sea sediments (d–f) micrometeorites collected from South Pole Water Well (SPWW) and Indian Ocean. The large relict grain stands clearly noticeable in the micrometeorites.

Figure 2.

Minor element (CaO, Al₂O₃, Cr₂O₃, MnO, FeO) of relict olivine from AMM in comparison with olivines of CI, CM and CV chondrites. The rectangle marked is the region where likelihood of finding the particle within it is maximum. The data for chondrites are taken from literature (Murray et al. 1986; Steele 1986, 1990; Kurat et al. 1989; Jones and Carey 2004; Russell et al., 2010; Rudraswami et al. 2011).

Figure 3.

Minor element (CaO, Al₂O₃, Cr₂O₃, MnO, FeO) of relict olivine from DSS in comparison with olivines of CI, CM and CV chondrites. The rectangle marked is the region where likelihood of finding the particle within it is maximum. The data for chondrites are taken from literature (Murray et al. 1986; Steele 1986, 1990; Kurat et al. 1989; Jones and Carey 2004; Russell et al., 2010; Rudraswami et al. 2011).

Figure 4.

Histogram plot of size of micrometeorites (top) and the relict grain (bottom) collected from Antarctica and Deep sea sediments.

Figure 5.

The distribution of percent of mass ablation for different size in diameter of entry particle over a range of ZA = 0° and 90° with entry velocities 11 and 16 km/s.

Figure 6.

Elemental ablation of Si, Mg and Fe for different size of particle over a range of ZA = 0° and 90°, for an entry velocity of 11 km/s. Ca, Al and Ti do not exhibit significant ablation hence are not included in the plot.

Figure 7.

Elemental ablation of Si, Mg, Fe, Ca, Al and Ti for different size of entry particle over a range of ZA = 0° and 90°, for an entry velocity of 16 km/s.

Figure 8.

Ternary diagram representing Mg-Si-Fe of different sizes of particles for ZA = 45° and 60° and entry velocities 11 and 16 km/s. A CI chondritic composition is used as the starting material.

Fig. 1

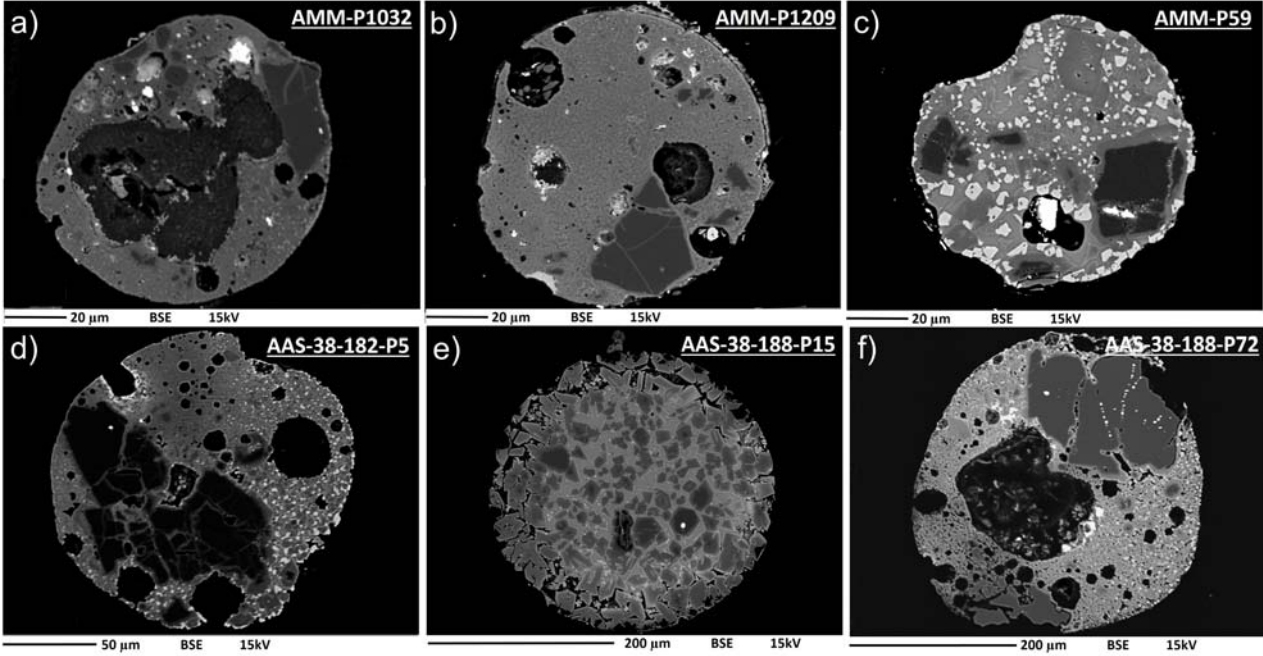


Fig. 2

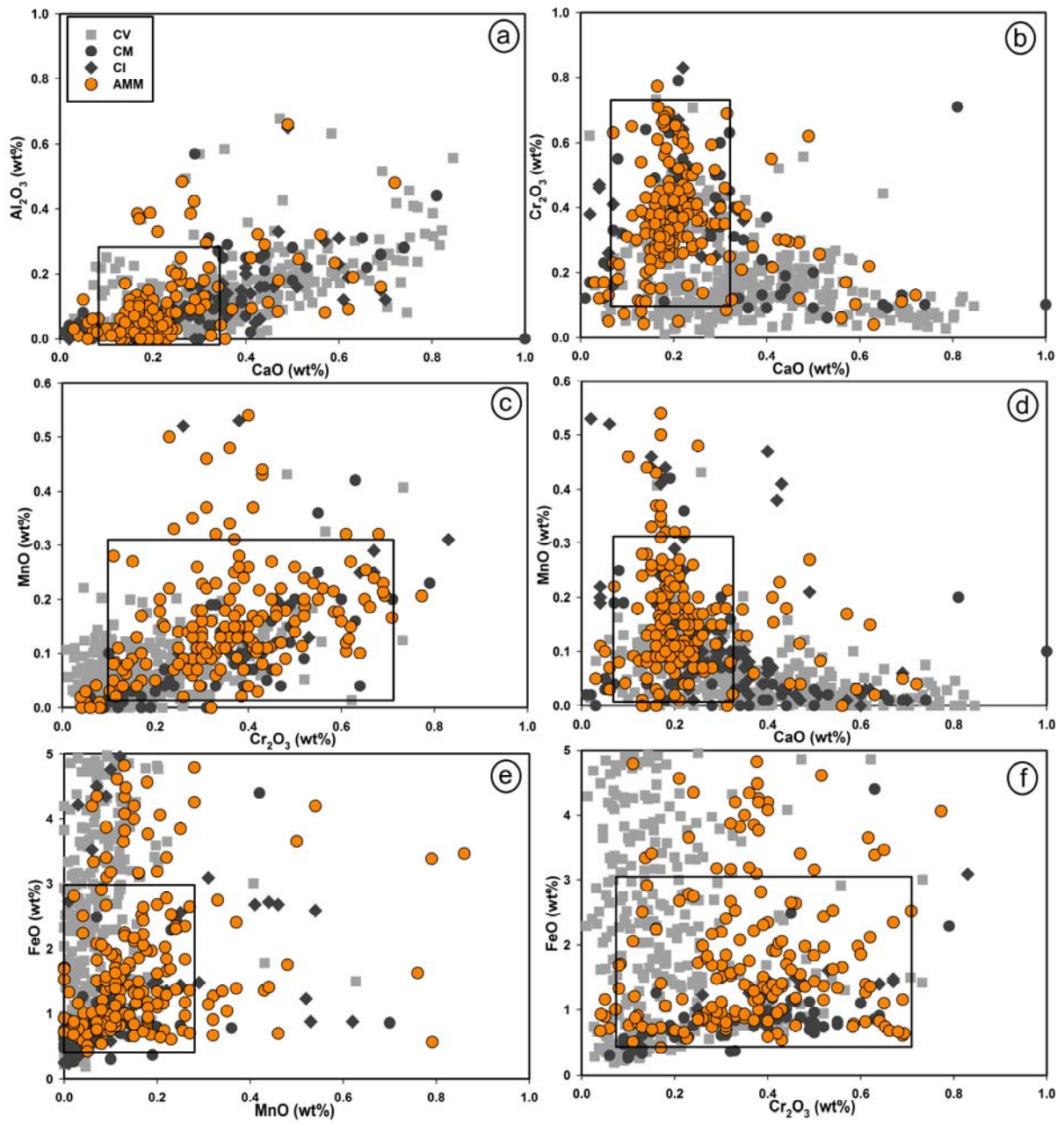


Fig. 3

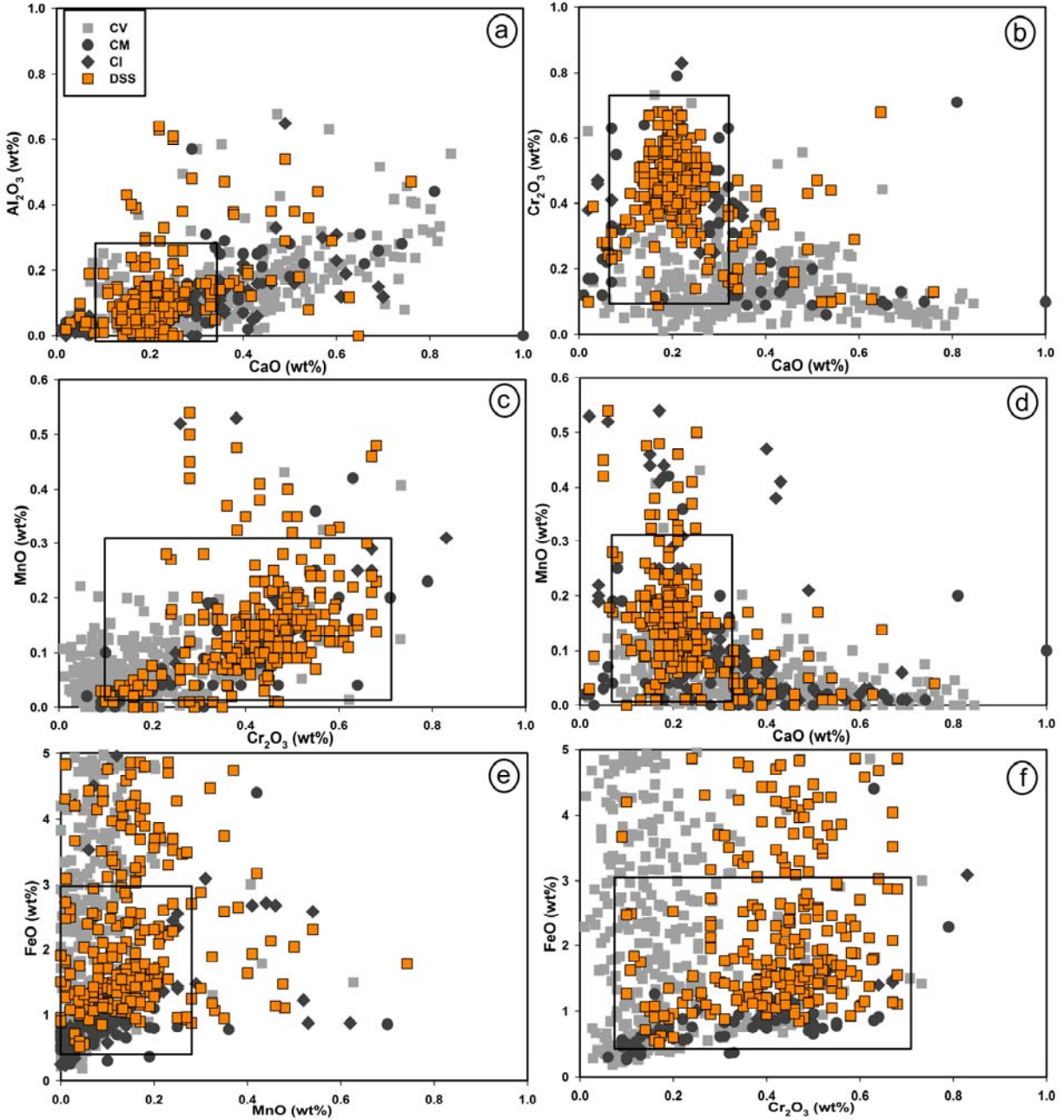


Fig.. 4

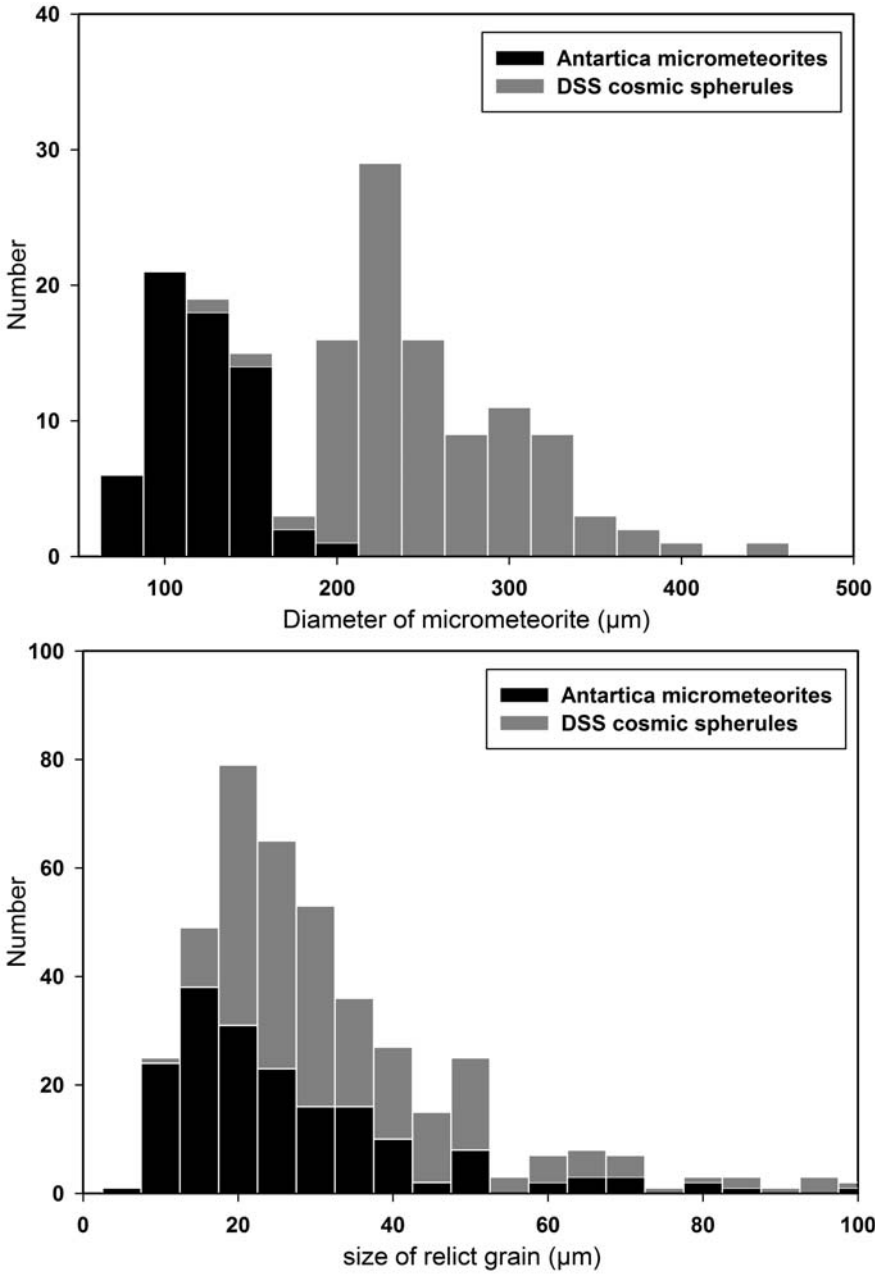


Fig. 5

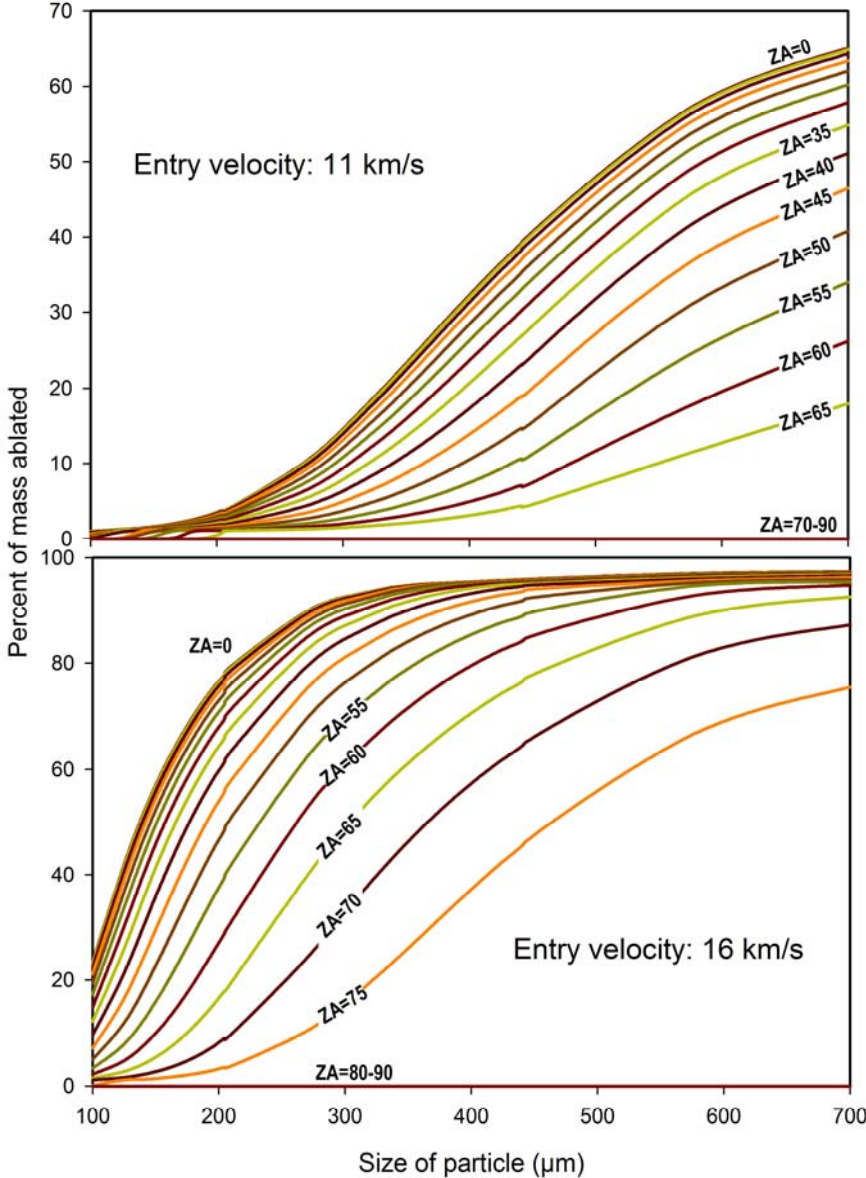


Fig. 6

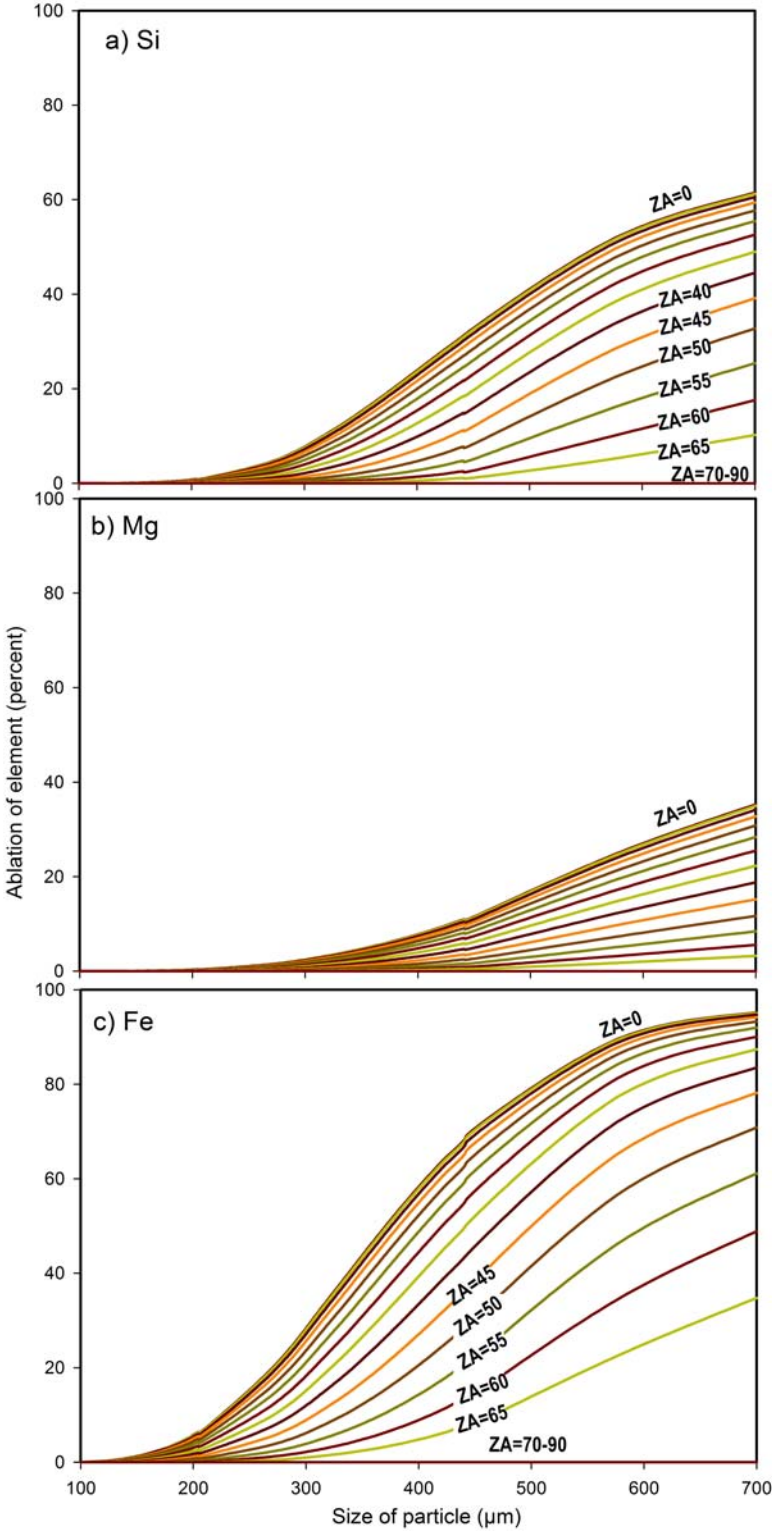


Fig. 7

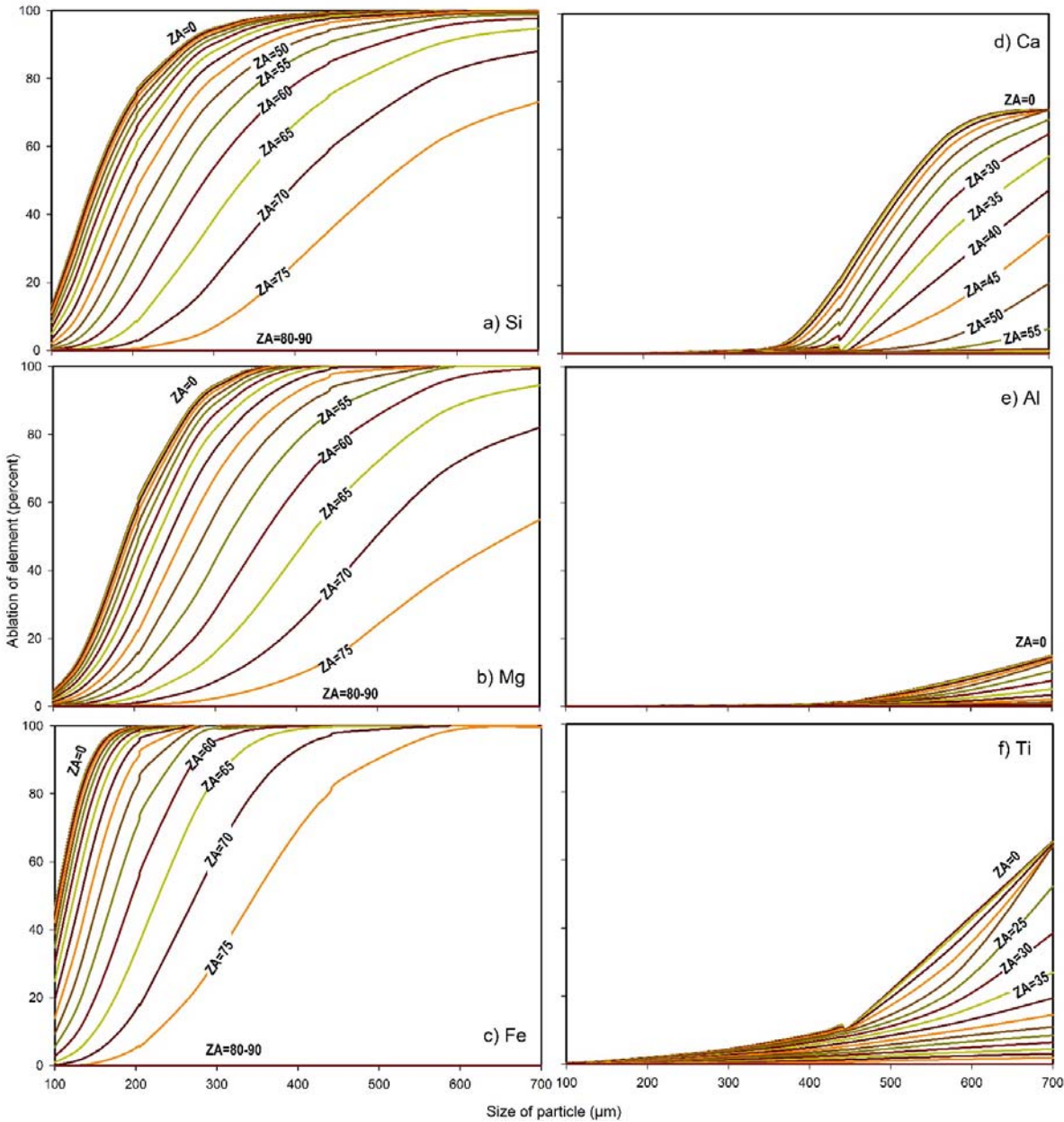


Fig. 8

